

Interactions of Cu(II) Ions with Framework Al in High Si:Al Zeolite Y as Determined from X- and W-Band Pulsed EPR/ENDOR Spectroscopies

Patrick J. Carl,[†] David E. W. Vaughan,[‡] and Daniella Goldfarb^{*,†}

Department of Chemical Physics, Weizmann Institute of Science, Rehovot, Israel 76100, and
Material Research Laboratory, Pennsylvania State University, State College, Pennsylvania

Received: December 18, 2001

A combination of continuous wave (CW) electron paramagnetic resonance (EPR), pulsed EPR, and pulsed electron–nuclear double resonance (ENDOR) techniques were used to obtain structural information about the Cu²⁺ ions in hydrated, room-temperature evacuated, and dehydrated Cu–Y (Si:Al = 12 and 5) with a particular emphasis on framework Al interactions. W-band ¹H ENDOR was used to probe the water ligands, whereas X-band hyperfine sublevel correlation (HYSCORE) spectroscopic measurements were employed to detect ²⁷Al hyperfine couplings. The X-band CW EPR spectra show that a total of three Cu²⁺ species (A, B, and C) are present in the samples. ENDOR measurements of hydrated and evacuated Cu–Y-12 indicate that species A and B have a complete coordination sphere of water and, on the basis of the absence of ²⁷Al signals in the HYSCORE spectrum, the Cu²⁺ is not directly bonded to the zeolite framework. Evacuation converted species B to species A. ¹H ENDOR spectra combined with simulations show that upon freezing, the equatorial and axial water ligands of species A and B have a distribution of orientations with respect to the Cu–O bond. The CW EPR spectrum of dehydrated Cu–Y-12 shows a single species (species C) and the HYSCORE spectrum exhibits cross-peaks from ²⁷Al with an isotropic coupling, *a*_{iso}, of 1.5 MHz. Unlike Cu–Y-12, evacuated Cu–Y-5 consists of species A and C, and the HYSCORE spectrum clearly shows a doublet of ²⁷Al cross-peaks with *a*_{iso} = 3.0 MHz assigned to species C. Upon dehydration, the ²⁷Al coupling decreases to 2.6 MHz. This indicates that in species C the Cu²⁺ is bound to framework oxygens which are bonded to an Al nucleus. For Si:Al = 5, the zeolite framework becomes negative enough that it can replace water ligands even after mild evacuation. Simulations of ²⁷Al HYSCORE spectra indicate that species C is Cu²⁺ bound to the framework oxygens primarily near a single Al nucleus with a large quadrupole coupling constant.

Introduction

Transition metal ion (TMI) supported catalysts are important both in environmental and synthetic chemistry. These heterogeneous catalysts are used in the production of fine chemicals and the decomposition of environmentally harmful chemicals. One class of these TMI catalysts that have received considerable attention because of their high catalytic activity are microporous materials, specifically aluminosilicate molecular sieves, namely, zeolites. The TMI and its local chemical environment within the support are important factors that influence the activity of these catalysts. Typically, in zeolites, there is more than one site which the TMI can occupy. The relative populations of these sites are influenced by the nature and the number of TMIs in the catalyst and the charge density within the zeolite, which is determined by the atomic Si:Al ratio. The chemistry of a TMI at a particular site is influenced by (1) limiting the possible coordination geometries, (2) altering the electronic properties of the TMI, and (3) limiting the access of reactant molecules to the TMI. A large amount of work has therefore been aimed at characterizing the various TMI sites present in these catalysts by various spectroscopic techniques.¹

One group of TMI catalysts which have received a considerable amount of attention are copper exchanged zeolites. These

catalysts have been shown to be active in the direct decomposition and selective catalytic reduction of nitrogen oxides (NO_x's, N₂O),^{2,3} the cyclodimerization of butadiene,⁴ the allylic oxidation of olefins,⁵ and the oxidative decomposition of benzene.⁶ To obtain information about the active catalytic site and the local structure of the copper cations in these catalysts, various spectroscopic techniques have been employed: X-ray absorption fine structure (XAFS),^{7,8} X-ray adsorption near edge (XANES),^{9,10} infrared (IR),¹¹ nuclear magnetic resonance (NMR),¹² and electron paramagnetic resonance (EPR)^{13–20} spectroscopies. Studies have shown that after aqueous Cu²⁺ exchanges, the Cu²⁺ cation has a full coordination shell of water and interacts weakly with the zeolite framework, and upon dehydration, the water ligands are lost and the Cu²⁺ cation coordinates with framework oxygen near framework Al (AlO₄[−]).^{13,16,17,21} To maintain the necessary charge balance, two situations are possible: (1) the Cu²⁺ cation either interacts with two framework Al's or (2) the Cu²⁺ cation interacts with one framework Al and with another anion present (for example an OH[−] ligand). A model based on divalent cations interacting with two Al has been developed by McAleer et al.²² and used to determine the maximum distance between Al's which the cations can bridge. These authors further postulated that as the Si:Al of the zeolite decreased the bridging distance of small cations (Ca²⁺) decreases because of the hydration shell about the cation. Furthermore, evidence from FTIR spectroscopy of Zn–ZSM-5²³ and EXAFS spectroscopy

* To whom correspondence should be addressed.

[†] Weizmann Institute of Science.

[‡] Pennsylvania State University.

of Fe–ZSM-5²⁴ suggest the catalytically active centers in these zeolites are associated with two framework Al's. However, direct evidence of the number of interacting Al's is not available.

Continuous wave (CW) EPR spectroscopy has been used extensively to provide information on the oxidation state, the identity, and the quantity of the Cu²⁺ centers in Cu-exchanged zeolites (X, Y, ZSM-5, beta, and ferrierite).^{15–18,20,25} In zeolite Y, the EPR parameters $g_{||}$ and $A_{||}$ have been interpreted on the basis of distinct sites within the faujasite structure;^{19,26} however, recent theoretical work has suggested that the EPR parameters are instead related to the number of Al atoms in the six-ring sites of the zeolite framework.²⁷ The information about the Cu²⁺ environment obtained from conventional CW EPR methods is limited because low resolution prevents the observation of the weak interaction between the unpaired electron and surrounding nuclei. Two EPR tools which have been useful for the direct observation of nearby nuclei in Cu²⁺ exchanged zeolites are electron spin echo envelope modulation (ESEEM) spectroscopy^{13,17,28} and electron nuclear double resonance (ENDOR) spectroscopy.^{29,30} Information on the local environment (identity of ligand atoms, distances of interacting nuclei, and coordination geometry) can be obtained using both ESEEM and ENDOR spectroscopies through the nuclear frequencies of nearby nuclei. Most ESEEM work has used the ²H modulations from deuterated adsorbates to probe the environment of the Cu²⁺ species present,^{13,14} whereas a few studies have used the ²⁷Al modulation.^{21,32,33} These studies detected ²⁷Al hyperfine coupling and used it to address the strength of Cu²⁺ binding to the framework and the location of Cu²⁺ in the zeolite X structure. The standard one-dimensional ESEEM spectra, however, suffer from distortions because of spectrometer dead time and tend to escape detection of broad lines,³² the two-dimensional (2D) ESEEM method, termed hyperfine sublevel correlation (HYSCORE) spectroscopy, is free of these drawbacks.³⁴

The presented work was motivated by the lack of direct information regarding the number of framework Al's which divalent cations interact with and the changes in this interaction with the Si:Al of the zeolite. Pulsed EPR techniques were used to probe in high detail the local environment of Cu²⁺ exchanged zeolite Y. In hydrated, evacuated, and dehydrated states, the orientation and distance of nearby ¹H nuclei (in water and/or hydroxide ligands) were probed using W-band (95 GHz) ENDOR experiments. X-band (~9 GHz) HYSCORE experiments were used to obtain information on the Cu²⁺ coordination to framework oxygens, via the ²⁷Al hyperfine interaction, as well as the number of framework Al in the near vicinity of the Cu²⁺ centers.

Materials and Methods

Sample Preparation. The parent zeolite (NaY Si:Al = 12 and 5) was obtained from Conteka B.V. The zeolite (1.5 g) was stirred with 100 mL of a 0.1 M sodium acetate (CH₃COONa·3H₂O, Merck) solution for 24 h with subsequent washing with 1 L of deionized water to give the Na⁺ form of the zeolite. Cu–Y was then prepared by stirring the Na⁺ form (0.200 g) with 25.00 mL of 0.2 mM copper nitrate (Cu(NO₃)₂·3H₂O, BDH Laboratory Supplies) for 24 h. The solution was filtered and washed with 1 L of deionized water and dried at room temperature for 24 h. If all of the Cu²⁺ in solution exchanged into the zeolite, the Cu:unit cell (UC) in the samples would be 0.4. Samples were subjected to three forms of treatment before spectroscopic measurements and the treatment cell used allowed for both X-band (3.0 mm OD) and W-band (0.9 mm OD) sample

tubes to be prepared simultaneously. (1) *Hydrated*, the as prepared sample was sealed in a quartz tube at room temperature and atmospheric pressure; (2) *Evacuated*, the sample was sealed in a quartz tube after evacuation at 10^{−3} Torr for 2 h; and (3) *Dehydrated*, the sample was evacuated at 10^{−3} Torr for 1 h, heated at 100 °C and 10^{−3} Torr for 1 h, and then the temperature was raised to 400 °C for 1 h. The sample was then exposed to 100 Torr of oxygen at 400 °C for 3 h to reoxidize Cu²⁺ that was reduced to Cu⁺. Finally, the sample was evacuated at 10^{−3} Torr and 400 °C for another hour to remove any adsorbed oxygen before cooling to room temperature and sealing under vacuum. The following naming convention will be used to identify the samples: *Treatment*-Cu–Y-Si:Al (Treatment: H = hydrated, E = evacuated, D = dehydrated, and Si:Al = 12 or 5).

Spectroscopic Measurements. CW EPR measurements were performed on a Varian E-12 spectrometer operating at X-band (~9.1–9.3 GHz). The magnetic field was calibrated with a DPPH standard placed in the cavity with the sample. All measurements were made at $T = 160$ K with a modulation amplitude of 5 G.

X-band pulsed EPR measurements were made at 8.7 GHz and 5 K on a home-built spectrometer.³⁵ Field-sweep echo detected (FS-ED) spectra were collected using the two pulse sequence ($\pi/2 - \tau - \pi - \tau$ - echo), where the echo intensity was recorded as a function of the magnetic field. In this experiment, microwave (MW) pulse lengths (t_{MW}) of 0.02 and 0.04 μ s with $\tau = 0.2$ μ s were employed. HYSCORE³⁴ spectra were recorded using the four pulse sequence ($\pi/2 - \tau - \pi/2 - t_1 - \pi - t_2 - \pi/2 - \tau$ - echo) and a four step phase cycle to remove the unwanted echoes.³⁶ The $\pi/2$ and π pulses used in these experiments were both 0.03 μ s, and τ 's of 0.20 and 0.24 μ s were employed (indicated in figure captions). The time domain data were processed, using MatLab,³⁷ as follows: the background echo decay in both t_1 and t_2 dimensions was removed by fitting to a high order polynomial followed by subtraction; both dimensions of the data were then convoluted with a Hamming function and zero filled to 512 points; a Fourier transformation (FT) was performed; and the magnitude spectrum was calculated.

W-band FS-ED EPR and ¹H ENDOR measurements were carried out at 94.9 GHz and 5 K on a home-built spectrometer.³⁸ FS-ED spectra were collected with t_{MW} of 0.06 and 0.12 μ s with $\tau = 0.3$ μ s. The magnetic field was calibrated using the ¹H Larmor frequency (ν_L) determined from the ENDOR spectra. The ¹H ENDOR spectra were measured using the Davies pulse sequence ($\pi - T - \pi/2 - \tau - \pi - \tau$ - echo with an RF pulse, t_{RF} , during the time T).³⁹ The experimental spectra were recorded with $t_{MW} = 0.3, 0.15,$ and 0.3 μ s, respectively, $\tau = 0.35$ μ s, $T = 15.0$ μ s, and $t_{RF} = 10.0$ μ s. The frequency scale of the experimental spectra is presented with respect to the nuclear Larmor frequency, ν_L , $\nu = \nu_{RF} - \nu_L$.

Spectral Simulations. The spin Hamiltonian for an $S = 1/2$ system interacting with n nuclei of spin I is

$$\hat{\mathcal{H}} = \beta \vec{B} \cdot \mathbf{g} \cdot \hat{S} + \sum_{i=1}^n [-g_N \beta_N \vec{B} \cdot \hat{I}_i + \hat{S} \cdot \hat{\mathbf{A}}_i \cdot \hat{I}_i + \hat{I}_i \cdot \mathbf{Q}_i \cdot \hat{I}_i] \quad (1)$$

The first and second terms are the electronic and nuclear Zeeman interactions, respectively, where \vec{B} is the external magnetic field. The last two terms correspond respectively to the hyperfine and quadrupole interactions. \mathbf{A}_i , \mathbf{Q}_i , and \vec{B} are given in the principal axis system of \mathbf{g} (x, y, z) where \mathbf{A}_i and \mathbf{Q}_i are described by

their three principle values, $A_{XX,i}$, $A_{YY,i}$, and $A_{ZZ,i}$ and $Q_{XX,i}$, $Q_{YY,i}$, and $Q_{ZZ,i}$. The Euler angles which transform from the principal axis systems of \mathbf{A}_i , \mathbf{Q}_i , and \mathbf{B} to the \mathbf{g} frame are

$$\begin{aligned}\mathbf{A}_i^P &\xrightarrow{\alpha_i, \beta_i, \gamma_i} \mathbf{A}_i^g \\ \mathbf{Q}_i^P &\xrightarrow{\alpha'_i, \beta'_i, \gamma'_i} \mathbf{Q}_i^g \\ \mathbf{B}^L &\xrightarrow{0, \theta, \phi} \mathbf{B}^g\end{aligned}\quad (2)$$

where the laboratory frame, L, is defined with Z in the direction of \mathbf{B} . For an axially symmetric \mathbf{g} tensor, the principal values are g_{\perp} and g_{\parallel} , and only two Euler angles are required (θ and ϕ) to transform the laboratory frame to the \mathbf{g} frame. An axially symmetric hyperfine interaction is usually described by an isotropic component, $a_{\text{iso},i}$, and an anisotropic component, $a_{\perp,i}$, and the principle values of \mathbf{A}_i become

$$\begin{aligned}A_{XX,i} &= A_{YY,i} = A_{\perp,i} = -a_{\perp,i} + a_{\text{iso},i} \\ A_{ZZ,i} &= A_{\parallel,i} = 2a_{\perp,i} + a_{\text{iso},i}\end{aligned}\quad (3)$$

Using the point-dipole approximation, $a_{\perp,i}$ becomes

$$a_{\perp,i} = \frac{\mu_0}{4\pi} \frac{g\beta g_{\text{IN}}\beta_{\text{N}}}{r_i^3 h} \quad (4)$$

where r_i is the electron–nuclear distance.

Similarly, the quadrupole tensor can be described in terms of the quadrupole coupling constant, $Qu = e^2Qq/h2I(2I-1)$, and the asymmetry parameter, η_i

$$Q_{ZZ,i} = \left(\frac{3e^2Qq}{4hI(2I-1)} \right)_i \quad \eta_i = \frac{Q_{XX,i} - Q_{YY,i}}{Q_{ZZ,i}} \quad (5)$$

The HSCORE simulations in this work are based on the Hamiltonian given in eq 1 and were obtained using the TRYSORE program.⁴⁰

For an $S = 1/2$ and $I = 1/2$ system with axial symmetry, the frequencies of the nuclear transitions ($\Delta M_S = 0$ and $\Delta M_I = 1$) observed in the HSCORE and ENDOR experiment are given by the following analytical expressions:

$$\begin{aligned}\nu_{\alpha} &= \left[\left(\frac{1}{2}A - \nu_L \right)^2 + \frac{1}{4}B^2 \right]^{1/2} \\ \nu_{\beta} &= \left[\left(-\frac{1}{2}A - \nu_L \right)^2 + \frac{1}{4}B^2 \right]^{1/2} \\ A &= a_{\perp}(3 \cos^2 \theta - 1) + a_{\text{iso}} \\ B &= 3a_{\perp} \sin \theta \cos \theta\end{aligned}\quad (6)$$

where θ is the angle between A_{ZZ} and the applied magnetic field.

To the first order, which is valid for ^1H at high fields such as 3 T, these frequencies are approximated by

$$\nu_{\alpha,\beta} = |-\nu_L \pm \frac{1}{2}A| \quad (7)$$

ENDOR simulations were obtained using a program developed in our group based on the theory of Erickson⁴¹ for $S = 1/2$ with

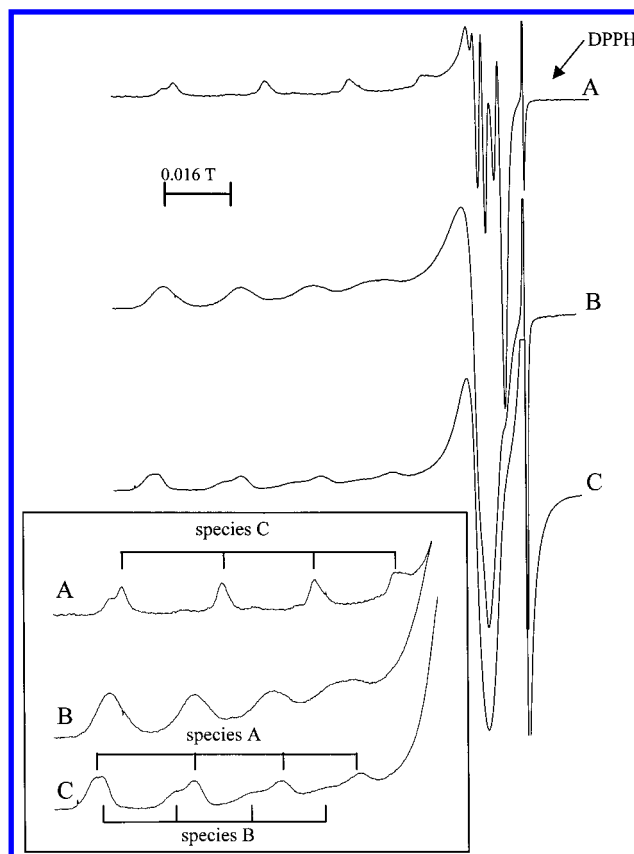


Figure 1. Low temperature (160 K) X-Band CW EPR spectra of (A) D-Cu-Y-12, (B) E-Cu-Y-12, and (C) H-Cu-Y-12. Inset: expansion of the parallel region from 0.214 to 0.312 T. The A_{\parallel} features of the different species are indicated in the inset.

n interacting nuclei as described by eq 1, where the quadrupole term is eliminated for ^1H 's (see eq 5).

Results

EPR. CW EPR spectra of Cu-Y-12 after the various treatments are presented in Figure 1. The spectra are typical of Cu^{2+} exchanged zeolites in the hydrated and dehydrated states.^{16–18} The spectrum of H-Cu-Y-12 (Figure 1C) shows two overlapping signals with considerable line broadening, resolved hyperfine features in the low field region (g_{\parallel} region) and no resolved hyperfine features in the high field region (g_{\perp} region). The two signals exhibit different degrees of g and A strain, an increase in the line broadening with field,⁴² which is clearly seen in the highest field hyperfine feature in the g_{\parallel} region of the spectrum. Evacuation of the sample (Figure 1B) caused the conversion of the minor signal in Figure 1C to the major signal resulting in a single signal which exhibits larger g and A strain. Dehydration resulted in the formation of a new signal (Figure 1A) where the perpendicular hyperfine features can be discerned and the two isotopes of Cu (^{65}Cu , 30.8% abundance and ^{63}Cu , 69.2% abundance) are resolved in the lowest field parallel hyperfine feature. CW EPR spectra of evacuated and dehydrated Cu-Y-5 (not shown) showed similar behavior to those of Cu-Y-12; however, two overlapping signals were present in both the evacuated and dehydrated spectra. The g and A values for the various signals were estimated from the spectra and are reported in Table 1. The different EPR signals are designated based on g_{\parallel} and A_{\parallel} as species A ($g_{\parallel} = 2.37$ – 2.39 , $A_{\parallel} = 430$ – 480 MHz), species B ($g_{\parallel} = 2.42$, $A_{\parallel} = 420$ MHz), and species C ($g_{\parallel} = 2.33$ – 2.34 , $A_{\parallel} = 500$ – 525 MHz).

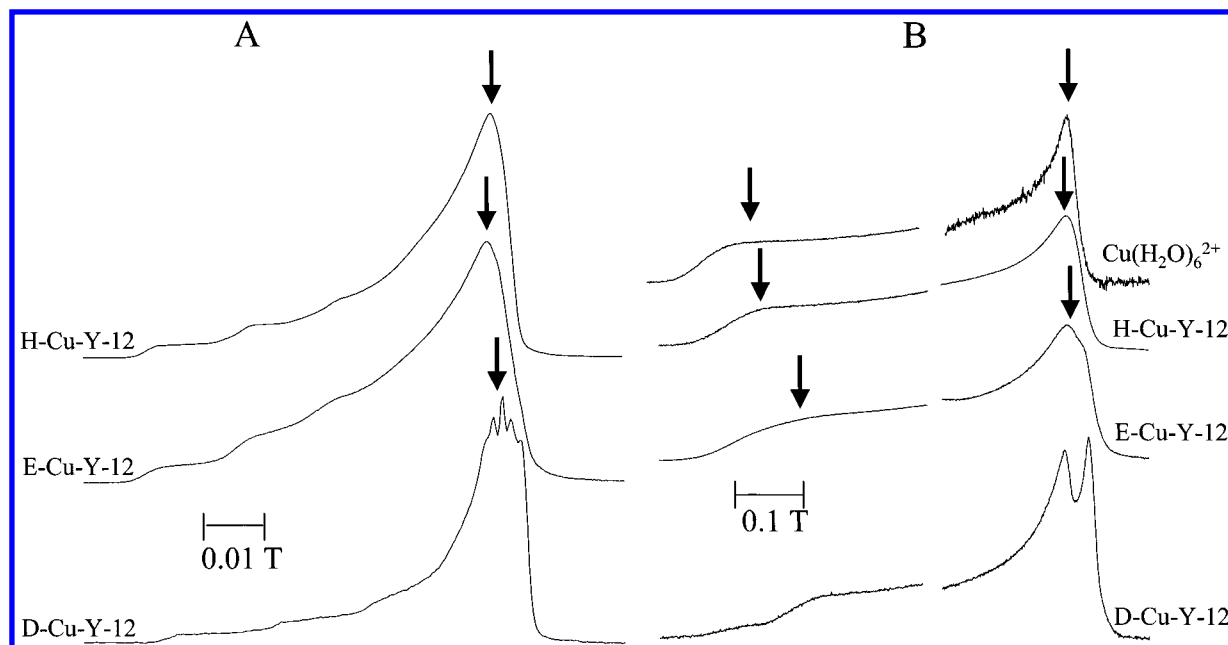


Figure 2. FS-ED EPR spectra: (A) X-band, field range 0.23–0.33 T, of H-Cu-Y-12, E-Cu-Y-12, and D-Cu-Y-12. (B) W-band, field range 2.75–3.35 T, of a 2 mM $\text{Cu}(\text{NO}_3)_2$ solution, H-Cu-Y-12, E-Cu-Y-12, and D-Cu-Y-12. Arrows indicate field positions where HYSCORE and ENDOR spectra were collected.

TABLE 1: EPR Parameters Determined from X-Band CW-EPR Spectra

sample	species designation	g_{\parallel} ± 0.01	$A_{\parallel}/\text{MHz (T)}$ $\pm 25 (\pm 0.0007)$	g_{\perp} ± 0.01
H-Cu-Y-12	A	2.39	481 (0.0144)	2.08
	B	2.42	420 (0.0124)	
E-Cu-Y-12	A	2.39	435 (0.0130)	2.08
D-Cu-Y-12	C	2.34	505 (0.0154)	2.06
	C	2.33	523 (0.0154)	
E-Cu-Y-5	A'	2.37	435 (0.0130)	2.08
	C	2.37	431 (0.0130)	
D-Cu-Y-5	A'	2.37	431 (0.0130)	2.08
	C	2.34	523 (0.0160)	

Prior to ENDOR and HYSCORE experiments, FS-ED EPR spectra were recorded to determine the field position at which these experiments would be performed. In the latter, the electron spin-echo intensity is measured as a function of the magnetic field, and the spectra are often similar to absorption CW EPR spectra. FS-ED EPR spectra are more sensitive to broad lines, they depend on the presence of nuclear modulations^{43,44} and on the relaxation of the paramagnetic species, both of which affect the echo intensity. Differences in the relaxation rates of the paramagnetic species can be used to edit the FS-ED spectra by changing the repetition rate of the pulse sequence. This results in slowly relaxing species contributing less to the echo intensity and allows the discrimination of overlapping spectra.

X- and W-band FS-ED EPR spectra are presented in Figure 2 A and B, respectively. The X-band FS-ED spectra show similar changes as the CW EPR spectra: an increase in line broadening on evacuation and a decrease in line broadening after dehydration. After the first derivative of the spectra (not shown) is taken and smoothed, the hyperfine features of the three species could be observed in the FS-ED spectra.

As the magnetic field and frequency are increased (W-band vs X-band), the ability to resolve species based on g values increases, whereas the hyperfine features are lost because this interaction does not scale with field, but the inhomogeneous broadening does increase because of g strain. The decrease in g_{\parallel} as the sample is evacuated and dehydrated can be clearly seen in the W-band FS-ED spectra (Figure 2 B). The signal of

species B observed at X-band in H-Cu-Y-12 is not resolved at W-band. The W-band FS-ED spectrum of E-Cu-Y-12 indicates the presence of two unresolved species; however, the FS-ED spectrum of D-Cu-Y-12 clearly shows two species resolved in both g_{\parallel} and g_{\perp} . The intensity of the lowest field signal was found to be dependent on the repetition rate of the pulse sequence (not shown) indicating a slower relaxing species. It should be noted that the gap in the data is due to an instrumental restriction. The spectrometer setup only allows a maximum field sweep of 0.4 T at once. The large field range of the W-band FS-ED spectrum required a setup change which left a small region of the magnetic field range (0.01 T) out of the sweep, because of some instrumental problem. The differences in noise level of each spectrum is a result of differences in the number of accumulations.

HYSCORE. The HYSCORE experiment correlates the nuclear (NMR) transitions of one electron spin manifold with the nuclear transitions of the other electron spin manifold. For example, for $S = 1/2$, $I = 1/2$, the $M_I = +1/2 \leftrightarrow -1/2$ transition in the $M_S = \alpha$ manifold, ν_{α} , is correlated with the $M_I = +1/2 \leftrightarrow -1/2$ transition in the $M_S = \beta$ manifold, ν_{β} . These correlations appear in the spectrum as off diagonal, cross-peaks with basic frequencies (ν_{α} , ν_{β}) and (ν_{β} , ν_{α}) (which are symmetric with respect to the diagonal) in (+, +) and (−, +) quadrants. The basic frequencies are centered about the nuclear Larmor frequency, ν_L , such that $(\nu_{\alpha} + \nu_{\beta})/2 \sim \nu_L$. These frequencies provide the identity of the nucleus through ν_L , whereas the hyperfine coupling of the nucleus is estimated by $A \sim \nu_{\alpha} - \nu_{\beta}$. Peaks along the diagonal in the experimental HYSCORE spectrum are often a result of incomplete inversion of the electron spin-echo by the π pulse and from weakly coupled nuclei where $\nu_{\alpha} \approx \nu_{\beta}$. For brevity, because the peaks in the HYSCORE spectra are symmetric, only one of the pair will be mentioned when discussing experimental and simulated spectra.

For nuclei with $I \geq 1$ (^2H , ^{27}Al , and ^{14}N), the experimental spectrum becomes more complicated because the number of nuclear states, M_I , increases, and the nuclear quadrupole effect becomes important. With more nuclear states present, higher order nuclear frequencies, corresponding to transitions with ΔM_I

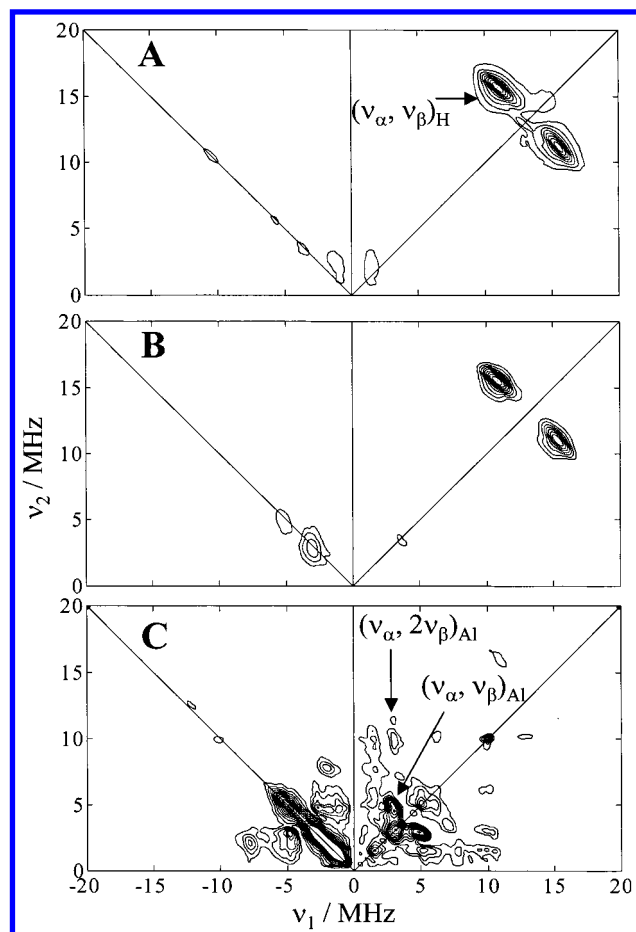


Figure 3. X-band HYSCORE spectra recorded with $\tau = 0.20 \mu\text{s}$ at g_\perp as indicated in Figure 2 A of (A) H-Cu-Y-12, (B) E-Cu-Y-12, and (C) D-Cu-Y-12.

$= 2, 3$, etc. become possible, and correlation between the two electron spin manifolds results in cross-peaks with frequencies $(n\nu_\alpha, m\nu_\beta)$ and $(m\nu_\alpha, n\nu_\beta)$, where n and $m = 1, 2, 3$. However, the intensity of these peaks decreases as m and/or n increase, so typically only single-double and double-double quantum transitions ($n = 1, 2$ and $m = 1, 2$) are observed in the experimental spectrum. Multiple frequencies of the type $(2\nu_\alpha, \nu_\beta)$ can also be observed in the spectrum when multiple nuclei are present. In the absence of any quadrupole effect, all single quantum nuclear transitions within an M_S manifold are equivalent and a single peak is observed in the HYSCORE spectrum. The nuclear quadrupole effect causes a shift in the energy level of each M_I , and the nuclear transitions become nonequivalent. The basic frequency peak, (ν_α, ν_β) , in the HYSCORE spectrum is then split into multiple peaks depending on the size of the quadrupole coupling constant and the asymmetry parameter (see eq 5).

X-band HYSCORE spectra of Cu-Y-12 and Cu-Y-5 samples were recorded at the field position corresponding to g_\perp (marked by arrow in FS-ED spectra in Figure 2A) and are presented in Figures 3 and 4, respectively. HYSCORE spectra of H-Cu-Y-12 and E-Cu-Y-12 (Figure 3 parts A and B) show a pair of ^1H cross-peaks at (10.9, 15.7) MHz, which corresponds to $(\nu_\alpha, \nu_\beta)_H$ (or $(\nu_\beta, \nu_\alpha)_H$), from which a maximum ^1H hyperfine coupling, A , of ~ 8 MHz was estimated. In Cu-Y-12, a minor decrease in the intensity of the ^1H peaks after evacuation of the hydrated sample occurred indicating a loss of waters of hydration. However, in both samples, no signal was present which could be attributed to ^{27}Al . Dehydration caused an almost complete elimination of the ^1H peaks (Figure 3C) and the

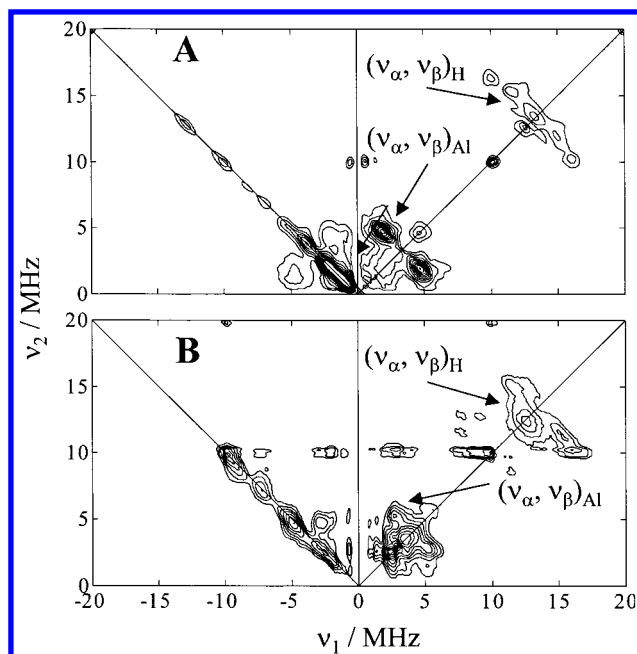


Figure 4. X-band HYSCORE spectra recorded at g_\perp of (A) H-Cu-Y-5 $\tau = 0.24 \mu\text{s}$ and (B) D-Cu-Y-5 $\tau = 0.20 \mu\text{s}$.

appearance of signals from ^{27}Al with major intensities at (3.0, 4.5) MHz corresponding to the basic frequencies $(\nu_\alpha, \nu_\beta)_{Al}$ with an estimated $A = 1.5$ MHz. Additional signals at (3.0, 9.9) MHz and (4.9, 6.1) MHz correspond to $(\nu_\alpha, 2\nu_\beta)$ and $(2\nu_\alpha, \nu_\beta)$, respectively. Signals appear also off the diagonal in the $(-, +)$ quadrant as expected for the intermediate coupling case, $A \sim \nu_L$.^{34,45} Peaks on the $(-, +)$ diagonal are noise.

The HYSCORE spectra of Cu-Y-5 reveal the difference in behavior of this sample as compared to Cu-Y-12. The spectrum of E-Cu-Y-5 (Figure 4A) shows ^1H ridges centered at (13.3, 13.3) MHz with a width of 8 MHz perpendicular to the diagonal. The difference in the shape of the ridges, as compared to that in E-Cu-Y-12 (Figure 4A) is attributed to the different τ used to record the spectra ($\tau = 0.20$ vs $0.24 \mu\text{s}$) and the τ suppression effect.⁴⁶ Clear ^{27}Al signals at (1.8, 4.8) MHz with an estimated $A = 3.0$ MHz were observed as well. In this case, the ^{27}Al peaks show no τ dependence at $\tau = 0.20$ and $0.24 \mu\text{s}$. ^{27}Al peaks arising from combination frequencies of the type $(\nu_\alpha, 2\nu_\beta)$ and $(2\nu_\alpha, \nu_\beta)$ were not observed. Although E-Cu-Y-12 showed no signals in this region, E-Cu-Y-5 exhibited very strong signals suggesting a strong interaction with ^{27}Al nuclei in this partially hydrated state. Dehydration resulted in few changes in the HYSCORE spectrum (Figure 4B). The ^{27}Al signals were still present, (2.7, 5.3) MHz, but A decreased to 2.6 MHz. A weak ridge of ^1H signals with a width of 6 MHz is present as well (the horizontal ridge at 10 MHz is due to noise). The significant ^1H signal intensity remaining after dehydration of Cu-Y-5 suggests incomplete dehydration, and a comparison to D-Cu-Y-12 shows a more complete loss of coordinating water molecules at Si:Al = 12 than at Si:Al = 5.

HYSCORE Simulations. In the present study, ^{27}Al peaks and combination frequencies can arise from the large nuclear spin, $I = 5/2$, the quadrupole effect, and the presence of multiple nuclei. To investigate the impact of these factors on the HYSCORE spectrum, spectral simulations were performed. Simulations (not shown) show that the peak positions are determined by the isotropic coupling, a_{iso} , while the width (perpendicular to the diagonal) of the peaks is determined by the anisotropic component, a_\perp , which is relatively small. The

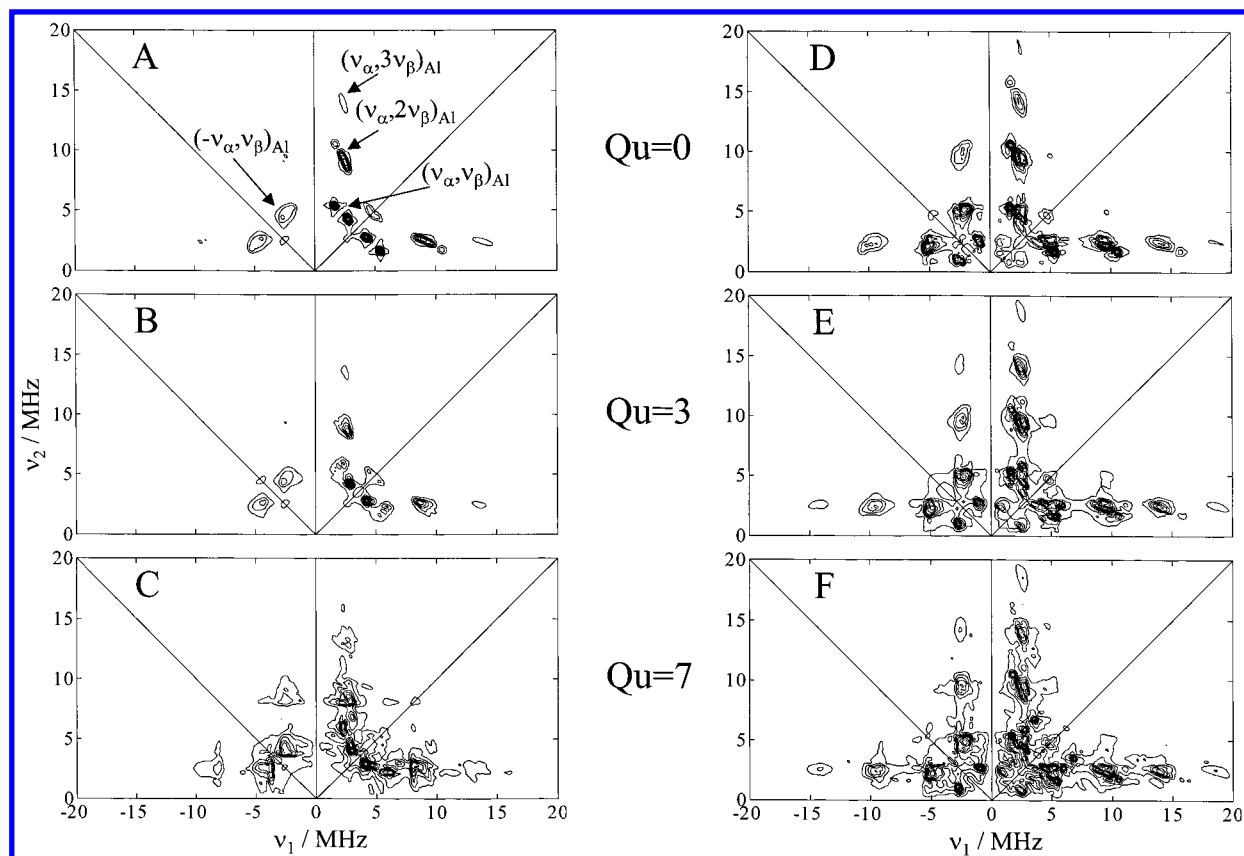


Figure 5. ^{27}Al HYSCORE simulations of (A–C) one Al and (D–F) two Al nuclei, where the quadrupole coupling constant (Q_u) is noted between the spectra. Simulation parameters for A–C: $a_{\text{iso}}=3.0$ MHz, $a_{\perp}=1.0$ MHz, $\alpha=0^\circ$, $\beta=50^\circ$, $\gamma=0^\circ$, $\eta=0.7$, $\alpha'=0^\circ$, $\beta'=50^\circ$, $\gamma'=0^\circ$, $g_{\perp}=2.08$, $g_{\parallel}=2.34$, $B_0=0.2995$ T, $\nu_{\text{MW}}=8.75$ GHz, $\theta=60\text{--}90^\circ$, $\phi=0\text{--}180^\circ$, and $\tau=0.2$ μs . D–F: same as A–C for two Al nuclei with the same parameters as above, and the second Al has $\gamma=60^\circ$.

ridge patterns are governed by the quadrupole coupling constant. The influence of the quadrupole coupling constant, Q_u , on the spectrum, for $a_{\text{iso}}=3$ MHz and $a_{\perp}=1$ MHz, is presented for a single ^{27}Al nucleus in Figure 5A–C. For $Q_u=0$, the single–single (2.5,4.5) MHz, single–double (2.5,9) (5,4.5) MHz, and single–triple (2.5,13) MHz correlations are observed, and the single–single peaks are split because of the τ dependence.⁴⁶ As Q_u increases, these peaks are split into multiple ridges resulting in an apparent broadening of each peak. Simulations of the HYSCORE spectrum with two similar ^{27}Al nuclei are presented in Figure 5D–F, where the two ^{27}Al nuclei are oriented as would be expected in the six-ring site of the faujasite structure (see figure caption). The most pronounced differences upon the inclusion of a second nucleus is the increase in intensity of peaks from multiple quantum transitions in both quadrants. Similar to the single nucleus simulations, increasing Q_u leads to splitting of the peaks present at $Q_u=0$ (Figure 5D).

The high resolution in the experimental spectrum of D–Cu–Y-12 (Figure 3C) allows the ridge patterns of the single–single quantum transitions as well as the single–double quantum transitions to be clearly observed. A comparison of both the single and double nuclei ^{27}Al HYSCORE simulations with the experimental spectrum shows similar peak positions for two cases: (1) an unpaired electron interacting with two similar Al nuclei with a moderate quadrupole coupling constant ($Q_u \approx 3$ MHz), Figure 5E or (2) an unpaired electron interacting with a single Al nucleus with a large quadrupole ($Q_u \approx 7$ MHz), Figure 5C. Both cases account for peak positions in the (+,+) quadrant as well as ridge patterns. In the (–,+) quadrant of the simulations, a broad peak appears at (–7.5,2.5) MHz in the single Al simulation, and a similar peak appears at (–9,2.5)

MHz in the double Al simulation. The experimental spectrum shows a peak in the (–,+) quadrant at (–7.7,2.2) MHz. This agreement in the (–,+) quadrant between the simulation (Figure 5C) and the experiment (Figure 3C) indicates a single Al nucleus interacting with the Cu^{2+} center in D–Cu–Y-12.

ENDOR. The ENDOR experiment records the NMR transitions of nuclei near the unpaired electron through changes in the intensity of the electron spin–echo imposed by the RF irradiation. For an orientationally disordered sample, further information on the orientation of the hyperfine tensor, **A**, with respect to the g tensor can be obtained using orientation selective ENDOR.^{47–49} By changing the field where the ENDOR spectrum is collected, different orientations of the paramagnetic center can be selectively probed with the ENDOR experiment. For systems with axial symmetry, setting the magnetic field at g_{\perp} will select paramagnetic centers with their symmetry axis perpendicular to the field, whereas setting the magnetic field at g_{\parallel} will select paramagnetic centers with their symmetry axis parallel to the field. The ENDOR line-shape variation within the EPR powder pattern then provides the orientation of the **A** tensor with respect to the g tensor which can then be translated into bond angles.

Information about nearby ^1H 's was obtained using W-band ^1H ENDOR. ENDOR spectra of a 2 mM $\text{Cu}(\text{NO}_3)_2$ solution, H–Cu–Y-12, and E–Cu–Y-12 at fields corresponding to g_{\perp} and g_{\parallel} (as indicated by arrows in the FS-ED spectra in Figure 2B) are presented in Figure 6. Not shown are the ENDOR spectra of the two species observed in the W-band FS-ED spectrum of D–Cu–Y-12, where the lower field species exhibits a spectrum similar to that in Figure 6A, whereas the higher field species does not exhibit an ENDOR effect. The $\text{Cu}(\text{NO}_3)_2$

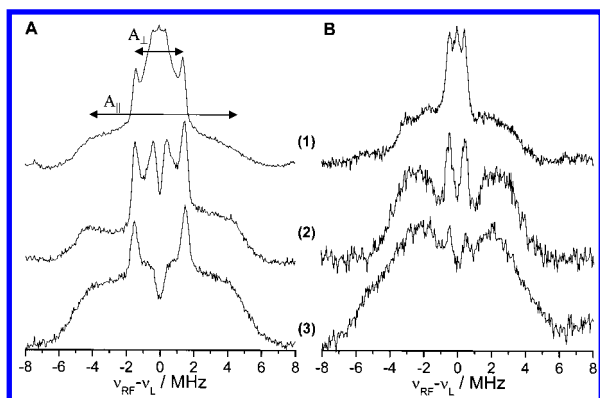


Figure 6. W-band ^1H ENDOR spectra recorded at (A) g_{\perp} as indicated in Figure 2A and at (B) $\sim g_{\parallel}$ indicated in Figure 2B of (1) a 2 mM $\text{Cu}(\text{NO}_3)_2$ solution, (2) H-Cu-Y-12, and (3) E-Cu-Y-12.

solution is used as a model solution for a completely hydrated Cu^{2+} complex, $\text{Cu}(\text{H}_2\text{O})_6^{2+}$. All three samples exhibit similar spectral features. Spectra recorded at g_{\perp} (Figure 6A) exhibit two powder patterns centered about the ^1H Larmor frequency. The first, with small splittings (<1 MHz), are due to remote ^1H nuclei from waters of solvation and they can be seen to decrease in intensity upon evacuation of the hydrated sample (Figure 6A trace 2 vs 3). The second shows singularities with splittings of ~ 3 and ~ 9 MHz corresponding to A_{\perp} and A_{\parallel} , respectively. The similarity in splittings of these powder patterns between the $\text{Cu}(\text{H}_2\text{O})_6^{2+}$ and H- and E-Cu-Y-12 suggests a similar orientation of the protons with respect to the Cu^{2+} center in all samples. Spectra recorded in the g_{\parallel} region (Figure 6B) also exhibit two doublets centered about the ^1H Larmor frequency, a broad doublet with splitting of ~ 5 MHz and a narrow doublet with splitting (<1 MHz). The doublets with splitting (<1 MHz) exhibit the same behavior as in the g_{\perp} region and are attributed to waters of solvation. The broad doublet with a splitting of ~ 5 MHz is observed in all three samples and is attributed to ligand water molecules.

ENDOR Simulations. To understand the orientation dependence of the ^1H ENDOR spectra, simulations of the spectra at both field positions and as a function of the ^1H position were performed. The orientation of the protons with respect to Cu^{2+} were based on an axially symmetric complex, where the orientation of the g tensor with respect to the molecular axis system is known. For axially symmetric copper complexes, the ligands are classified as equatorial (in the xy plane) and axial (along z axis) where the g tensor and the molecular axes coincide.⁵⁰ The position of the ^1H nucleus can then be described by two angles: ψ , the angle between the A_{zz} and the g_{\parallel} direction, and φ , the azimuthal angle of A_{zz} .

Initially, we considered a simple model of a single ^1H at a distance of 2.7 \AA ($a_{\text{iso}} = 1.0 \text{ MHz}$ and $a_{\perp} = 3.8 \text{ MHz}$) and calculated the spectrum as a function of ψ as shown in Figure 7. For axial g and A tensors, the ENDOR spectrum of a single ^1H nucleus depends only on ψ . For an axial coordination environment (tetragonal, square pyramidal, or square planar), the ^1H ENDOR spectrum is composed of contributions from the axial ligands and the equatorial ligands. The simulations illustrate the effect of the ^1H position, with respect to g_{\parallel} and the molecular z axis, on the ENDOR spectra in both the g_{\perp} (Figure 7A) and the g_{\parallel} region (Figure 7B) of the EPR spectrum. Comparison with experimental spectra (Figure 6) indicates that a distribution of orientations is necessary to accurately represent the experimental spectra. In the g_{\perp} region of the EPR spectrum, orientation of the proton near the molecular xy plane, $\psi = 60\text{--}90^\circ$, approximates the powder patterns observed in Figure 6A,

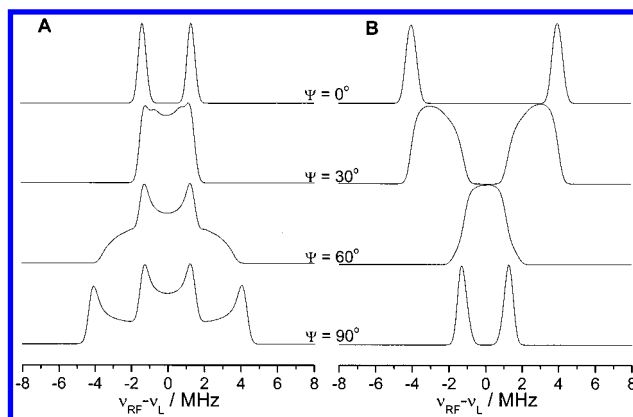


Figure 7. Simulations of ^1H W-band ENDOR spectra with $a_{\text{iso}} = 1.0 \text{ MHz}$ and $a_{\perp} = 3.8 \text{ MHz}$. (A) Magnetic field set at g_{\perp} ($\theta = 80\text{--}90^\circ$, $B_0 = 3.2517 \text{ T}$) and (B) magnetic field set to g_{\parallel} ($\theta = 0\text{--}20^\circ$, $B_0 = 2.8865 \text{ T}$) where the angle ψ is noted on the figure. Simulation parameters: $g_{\perp} = 2.08$, $g_{\parallel} = 2.39$, $\nu_{\text{MW}} = 94.9 \text{ GHz}$, $\nu_{\text{RF}} = 129\text{--}149 \text{ MHz}$, and $\phi = 0\text{--}180^\circ$.

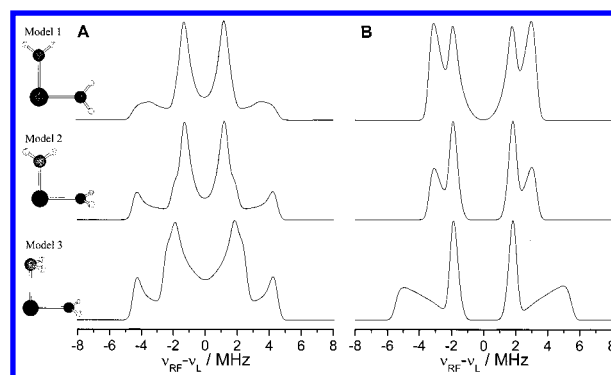


Figure 8. Simulations showing the effect of rotation of the equatorial and axial water ligands about Cu-O axis on the W-band ENDOR spectrum. (A) Magnetic field set at g_{\perp} , $\theta = 80\text{--}90^\circ$ and (B) magnetic field set to g_{\parallel} , $\theta = 0\text{--}20^\circ$. Pictures illustrate the orientation of the equatorial water molecules' protons of: (1) equatorial H's above and below molecular xy plane and axial H's perpendicular to molecular xy -plane, (2) equatorial H's in molecular xy plane and axial H's perpendicular to molecular xy plane, and (3) equatorial H's in molecular xy plane and axial H's parallel to molecular xy plane.

whereas in the g_{\parallel} region, an orientation tilted from the molecular z axis, $\psi = 30^\circ$, more closely approximates the powder patterns in Figure 6B. This orientation dependence of the ENDOR spectra supports the presence of axial water ligands about the Cu^{2+} center within the zeolite because protons of axial water can reach $\psi = 30^\circ$.

To further investigate the orientation of the water ligands, ^1H ENDOR simulations were performed using a model of three water ligands coordinated to the Cu^{2+} center. A diagram of the models used and the resulting ENDOR spectra in the g_{\perp} (A) and g_{\parallel} regions (B) are presented in Figure 8. The orientation of the water molecules was changed with respect to the molecular axis system where Cu-O bond lengths were taken to be 2.28 and 1.96 \AA for the axial and equatorial oxygens,³⁰ respectively, with an O-H bond length of 0.985 \AA and H-O-H angle of 104.5° . After the three water molecules were oriented, eq 4 was used to calculate $a_{i\perp}$ for each ^1H . The simulation parameters for each ^1H are summarized in Table 2. It can be seen from the various simulations that model 2 with the equatorial water ligands in the molecular xy plane and the axial water ligand perpendicular to the molecular xy plane agrees the best with the experimental spectra in Figure 6. The orientation of the equatorial ligands (Figure 8 models 1 and 2) can be observed

TABLE 2: ENDOR Simulation Parameters for Multiple Water Ligands

	axial water		equatorial water 1		equatorial water 2	
	H-1	H-2	H-3	H-4	H-5	H-6
Model 1						
$a_{\text{iso}}/\text{MHz}$	0.4	0.4	0.4	0.4	0.4	0.4
a_{\perp}/MHz	3.09	3.09	4.29	4.29	4.29	4.29
$r/\text{\AA}$	2.94	2.94	2.64	2.64	2.64	2.64
ψ	15.1	15.1	106.9	73.1	106.9	73.1
ϕ	0	180	0	0	90	90
Model 2						
$a_{\text{iso}}/\text{MHz}$	0.4	0.4	0.4	0.4	0.4	0.4
a_{\perp}/MHz	3.09	3.09	4.29	4.29	4.29	4.29
$r/\text{\AA}$	2.94	2.94	2.64	2.64	2.64	2.64
ψ	15.1	15.1	90	90	90	90
ϕ	0	180	-16.9	16.9	73.1	106.9
Model 3						
$a_{\text{iso}}/\text{MHz}$	0.4	0.4	0.4	0.4	0.4	0.4
a_{\perp}/MHz	5.37	5.37	4.29	4.29	4.29	4.29
$r/\text{\AA}$	2.45	2.45	2.64	2.64	2.64	2.64
ψ	23.4	23.4	90	90	90	90
ϕ	232.3	127.8	-16.9	16.9	73.1	106.9

to alter the powder pattern in the g_{\perp} region more than the g_{\parallel} region and vice versa for the orientation of the axial ligand (Figure 8 models 2 and 3). However, in the g_{\parallel} region, the experimental spectra do not show discrete peaks as do the simulations, which indicates that a distribution of different angles for the equatorial is present in the frozen samples. Similar is observed for the axial ligands.

Discussion

In the present study, the interaction with framework Al and the coordination environment of Cu^{2+} ions exchanged into zeolite Y was studied using pulsed EPR and ENDOR methods. Three distinct Cu^{2+} species were identified in samples of Cu-Y-12 and Cu-Y-5 by CW EPR experiments. Two of these species (A and B) are present in the hydrated and the evacuated samples, whereas the third species (C) is present in evacuated and dehydrated samples. The Cu^{2+} -framework interaction of these species was probed directly via the ^{27}Al hyperfine interaction, whereas coordination to water and/or hydroxide molecules was probed via the ^1H hyperfine couplings.

The CW-EPR spectra of the hydrated and evacuated samples show an increase in line broadening of the hyperfine features with field. This systematic broadening with M_I is attributed to g and A strain and provides indirect information about the Cu^{2+} complex interaction with the zeolite framework. g and A strain in Cu^{2+} complexes has been interpreted as resulting from a random distribution of bonding parameters produced upon freezing in glassy matrices.^{42,51} In zeolites, strain has been interpreted as being a measure of the heterogeneity of the Cu^{2+} sites present and the degree of interaction of the Cu^{2+} with the framework.²⁵ Both species observed in H-Cu-Y-12 exhibited an amount of g and A strain. Species B, the minor species, exhibited a higher degree of g and A strain when compared to species A, suggesting weaker interactions with the zeolite framework. Species A and B then correspond to Cu^{2+} complexes with weak interactions with the zeolite framework, such as $\text{Cu}(\text{H}_2\text{O})_6^{2+}$. On the basis of the W-band ^1H ENDOR spectra and simulations, the heterogeneity in the Cu^{2+} complexes which leads to the observed g and A strain is a result of the freezing process which leads to a distribution of orientations of the water ligands about similar Cu^{2+} centers. Both the CW EPR spectra and the ^1H ENDOR spectra agree that the water molecules coordinated to Cu^{2+} in hydrated and evacuated Cu-Y are

oriented with a distribution of angles with respect to the molecular axes, similar to that formed in $\text{Cu}(\text{H}_2\text{O})_6^{2+}$ in frozen solution.

Upon evacuation, species B is converted to species A as indicated in Figure 1 by the loss of the species B signal and the increase in the species A signal. This behavior along with the higher degree of g and A strain indicates species B has a larger water solvation shell and thus a weaker interaction with the framework. Evacuation removes these physisorbed waters and results in an increase in the interaction with the framework. The loss of water molecules is supported by ^1H ENDOR spectra of the hydrated and evacuated samples (Figure 6 parts A and B) where the smallest coupling ^1H signal decreases after evacuation. These small couplings appear in ENDOR spectra recorded in both the g_{\perp} and g_{\parallel} regions of the FS-ED spectrum indicating these signals are not due to either axially or equatorially coordinated water because they show no orientation dependence. Furthermore, the measured a_{\perp} of 0.9 MHz corresponds to a distance of 4.5 Å from eq 4, which is too distant to be considered as arising from a coordinated water molecule.

While CW EPR and ^1H ENDOR spectra do not give direct evidence of the Cu^{2+} -framework Al interaction, X-band HYSCORE spectra do. The HYSCORE spectra of hydrated and evacuated Cu-Y-12 show no peaks that are due to ^{27}Al nuclei (Figure 3 parts A and B). Species A and B, which are present in both states, are assigned as Cu^{2+} aquo complexes which are free of direct framework interaction and are situated in the larger α cage of the zeolite.

Interaction with framework Al is clearly visible in the HYSCORE spectrum of Cu-Y-12 after dehydration (Figure 3C). The presence of an ^{27}Al isotropic hyperfine coupling indicates a direct bonding of the Cu^{2+} center to the framework with significant spin density at the Al nucleus. The number of interacting Al nuclei is determined by comparison of the experimental spectrum with the HYSCORE simulations, where the peak positions are strongly dependent on the quadrupole coupling constant of the Al. The best agreement was found between experimental and simulated spectra for the single Al with $Q_u = 7$ (Figure 5C). The quadrupole coupling constant of ^{27}Al in dehydrated zeolites has been measured to be 4–6 MHz in NaY and NaZSM-5⁵² and 10–16 MHz in HX, HY, and HZSM-5.^{52,53} The Cu^{2+} species present, identified from CW EPR spectra as species C, can therefore be assigned as Cu^{2+} which is bound to a framework oxygen near a single Al nucleus with a large quadrupole coupling constant ($Q_u \approx 7$). W-band ^1H ENDOR spectra of this species were acquired and indicated no nearby ^1H 's, which suggest that no charge compensating hydroxide ligand is present as was observed in Cu-ZSM-5 using three-pulse ESEEM experiments.¹³

The CW EPR spectra of E-Cu-Y-5 and D-Cu-Y-5 indicate that two species, A' and C, are present. Species A', attributed to $\text{Cu}(\text{H}_2\text{O})_6^{2+}$, appears because of incomplete dehydration of the zeolite. Unlike Cu-Y-12, the HYSCORE spectrum of evacuated Cu-Y-5 shows peaks that are due to ^{27}Al (Figure 4A) attributed to species C. The spectrum did not show features from quadrupole effects; higher order transitions (single-double) were absent; and comparison with the HYSCORE simulations shows good agreement with Figure 5A, where the multiple frequencies are weaker relative to the basic frequencies. The lower quadrupole coupling is expected in the evacuated sample because of the presence of water.⁵⁴ This shows that the ability of the framework to act as a ligand of Cu^{2+} changes as the Al content increases. At Si:Al = 12, the zeolite oxygens are weaker ligands than water, and no interaction with frame-

work Al is observed. At Si:Al = 5, the situation changes, and zeolite oxygen replaces water ligands even after mild evacuation at room temperature. This change in coordinating strength of the framework may help explain how the Si:Al of the parent zeolite influences the catalytic activity.

In D-Cu-Y-5, as in D-Cu-Y-12, a substantial interaction with ^{27}Al was observed, again attributed to species C. Here, the spectrum did not exhibit clear high order peaks probably because of the lower quality of the HYSCORE spectrum. On the basis of simulations, the changes observed in the line-shape and splitting because of dehydration are attributed primarily to an increase in the ^{27}Al quadrupole coupling as water is removed. In this sample, the ^{27}Al quadrupole coupling is smaller than in D-Cu-Y-12. A concomitant, small change in the hyperfine coupling cannot be ruled out. The observed hyperfine coupling includes contributions from through bond interactions (isotropic coupling, Fermi contact) and through space interactions (dipole-dipole interactions). For a tetragonal Cu^{2+} complex, the unpaired electron resides in the $d_{x^2-y^2}$ orbital. When forming a tetragonal complex bound to the framework, this Cu orbital overlaps with the orbitals of framework oxygen in equatorial ligand positions. Transfer of spin density through the oxygens then results in spin density at the Al nucleus. If the geometry of this complex distorts from planar, the overlap of these orbitals would decrease, and spin density at the Al nucleus would therefore decrease. The loss of spin density at the Al nucleus would be reflected as a decrease in the isotropic coupling, a_{iso} .

Using a simple model of a random distribution of Al in the six rings, there is only a ~6% probability of finding a six ring having two Al's at Si:Al = 12. At low Cu^{2+} loadings, the majority of Cu^{2+} would therefore interact only with a single framework Al unless it has a preference for rings with two Al's. At Si:Al = 5, the probability of two Al's in one six ring increases to ~22%, which is still relatively low. If Cu^{2+} preferentially populates six rings with two Al's, a significant number of interactions with two framework Al's would be expected at low Cu^{2+} loadings. In this work, the Cu^{2+} species at both Si:Al = 12 and 5 were found to interact strongly with primarily a single framework Al, and no evidence of a substantial number of two Al interactions was observed. This does not rule out the possibility of Cu^{2+} interacting in an electrostatic/dipole manner with a remote Al ($>4 \text{ \AA}$ away).²² Such an interaction would result in very shallow modulation depths and consequently a weak peak centered on the diagonal in the HYSCORE spectrum. The CW EPR parameters of species C ($g_{\parallel} = 2.34$ and $A_{\parallel} = 435 \text{ MHz}$) are similar to those previously reported for dehydrated Cu-NaX and Cu-KX.²¹ There, using a combination of ^{27}Al ESEEM and earlier CW EPR,⁵⁵ this species was assigned to Cu^{2+} at site III or III' in the supercage.²¹

Conclusions

A combination of W-band ^1H ENDOR and X-band HYSCORE spectroscopies has provided direct evidence of the coordination environment of Cu^{2+} exchanged in zeolite Y. At low Al content (Si:Al = 12), two similar Cu^{2+} complexes have been identified in hydrated and evacuated samples and assigned to $\text{Cu}(\text{H}_2\text{O})_6^{2+}$ complexes located in the larger α cage. The two complexes show different strengths of interaction with the zeolite framework where the weakly interacting complex has a larger hydration shell about the Cu^{2+} center. In both complexes, the water ligands were found to be orientationally disordered with respect to the Cu-O bond. In the dehydrated state, Cu^{2+} was observed to bond directly to the oxygens of a single framework Al, placing significant unpaired electron spin density at the Al

nucleus, and no evidence for OH^- ligands in any of the species was observed. At a higher framework charge density (Si:Al = 5), Cu^{2+} was bonded to the framework after evacuation at room temperature, whereas at a low framework charge density (Si:Al = 12), Cu^{2+} was bonded to the framework only after dehydration. This bonding dependence on Si:Al of the zeolite shows that the zeolite oxygens become competitive ligands for Cu^{2+} after a specific framework charge density is achieved.

Acknowledgment. This work was supported by the Israel-USA Binational Science Foundation (BSF). Dr. Carl's research at the Weizmann Institute of Science is being supported by the Harry K. Stone Postdoctoral Fellowship.

References and Notes

- (1) Weckhuysen, B. M.; der Voort, P. V.; Catana, G., Eds.; *Spectroscopy of Transition Metal Ions on Surfaces*; Leuven University Press: Leuven, Belgium, 2000.
- (2) Centi, G.; Perathoner, S. *Appl. Catal. A* **1995**, *132*, 179.
- (3) Ganemi, B.; Björnborn, E.; Demirel, B.; Paul, J. *Microporous Mesoporous Mater.* **2000**, *38*, 287.
- (4) Voskoboinikov, T. V.; Coq, B.; Fajula, F.; Brown, R.; McDougall, G.; Couturier, J. L. *Microporous Mesoporous Mater.* **1998**, *24*, 89.
- (5) Carloni, S.; Frullanti, B.; Maggi, R.; Mazzacani, A.; Bigi, F.; Sartori, G. *Tetrahedron Lett.* **2000**, *41*, 8947.
- (6) Becker, L.; Förster, H. *Appl. Catal. B* **1998**, *17*, 43.
- (7) Yamashita, H.; Matsuoka, M.; Tsuji, K.; Shioya, Y.; Anpo, M.; Che, M. J. *Phys. Chem.* **1996**, *100*, 397.
- (8) Lamberti, C.; Bordiga, S.; Salvalaggio, M.; Spoto, G.; Geobaldo, F.; Vlaic, G.; Bellatreccia, M.; Zecchina, A. *J. Phys. Chem. B* **1997**, *101*, 344.
- (9) Lamberti, C.; Spoto, G.; Scarano, D.; Paze, C.; Salvalaggio, M.; Bordiga, S.; Zecchina, A.; Palomino, G. T.; D'Acapito, F. *Chem. Phys. Lett.* **1997**, *269*, 500.
- (10) Bordiga, S.; Zecchina, A.; Marra, G. L.; Palomino, G. T.; Lamberti, C. *J. Phys. Chem. B* **2000**, *104*, 8641.
- (11) Henriques, C.; Ribeiro, M. F.; Abreu, C.; Murphy, D. M.; Poignant, F.; Saussey, J.; Lavalley, J. C. *Appl. Catal. B* **1998**, *16*, 79.
- (12) Hu, S.; Reimer, J. A.; Bell, A. T. *J. Phys. Chem. B* **1997**, *101*, 1869.
- (13) Park, S.-K.; Kurshev, V.; Luan, Z.; Lee, C. W.; Kevan, L. *Microporous Mesoporous Mater.* **2000**, *38*, 255.
- (14) Yu, J.-S.; Comets, J.-M.; Kevan, L. *J. Phys. Chem.* **1993**, *97*, 11047.
- (15) Dědeček, J.; Sobalík, Z.; Tvarůžková, Z.; Kaucký, D.; Wichterlová, B. *J. Phys. Chem.* **1995**, *99*, 16327.
- (16) Attfield, M. P.; Weigel, S. J.; Cheetham, A. K. *J. Catal.* **1997**, *170*, 227.
- (17) Anderson, M. W.; Kevan, L. *J. Phys. Chem.* **1987**, *91*, 4174.
- (18) Larsen, S. C.; Aylor, A.; Bell, A. T.; Reimer, J. A. *J. Phys. Chem.* **1994**, *98*, 11533.
- (19) Schoonheydt, R. A. *Catal. Rev.-Sci. Eng.* **1993**, *35*, 129.
- (20) Oliva, C.; Selli, E.; Ponti, A.; Correale, L.; Solinas, V.; Rombi, E.; Monaci, R.; Forni, L. *J. Chem. Soc., Faraday Trans.* **1997**, *93*, 2603.
- (21) Goldfarb, D.; Zukerman, K. *Chem. Phys. Lett.* **1990**, *171*, 167.
- (22) McAleer, A. M.; Rees, L. V. C.; Nowak, A. K. *Zeolites* **1991**, *11*, 329.
- (23) El-Malki, E.-M.; Santen, R. A. V.; Sachtler, W. M. H. *J. Phys. Chem. B* **1999**, *103*, 4611.
- (24) Marturano, P.; Drozdová, L.; Kogelbauer, A.; Prins, R. *J. Catal.* **2000**, *192*, 236.
- (25) Carl, P. J.; Larsen, S. C. *J. Phys. Chem. B* **2000**, *104*, 6568.
- (26) Kevan, L. *Rev. Chem. Intermed.* **1987**, *8*, 53.
- (27) Pierloot, K.; Delabie, A.; Groothaert, M. H.; Schoonheydt, R. A. *Phys. Chem. Chem. Phys.* **2001**, *3*, 2174.
- (28) Böhlmann, W.; Pöpl, A.; Michel, D. *Colloids Surf.* **1999**, *158*, 235.
- (29) Biglino, D.; Li, H.; Erickson, R.; Lund, A.; Yahiro, H.; Shiotani, M. *Phys. Chem. Chem. Phys.* **1999**, *1*, 2887.
- (30) Li, H.; Biglino, D.; Erickson, R.; Lund, A. *Chem. Phys. Lett.* **1997**, *266*, 417.
- (31) Yu, J.-S.; Kim, J. Y. *Catal. Today* **1998**, *44*, 81.
- (32) Matar, K.; Goldfarb, D. *J. Phys. Chem.* **1992**, *96*, 3100.
- (33) Levi, Z.; Matar, K.; Raitisimring, A. M.; Goldfarb, D. *Pure and Appl. Chem.* **1992**, *64*, 799.
- (34) Höfer, P.; Grupp, A.; Nebenführ, H.; Mehring, M. *Chem. Phys. Lett.* **1986**, *132*, 279.
- (35) Shane, J. J.; Gromov, I.; Vega, S.; Goldfarb, D. *Rev. Sci. Instrum.* **1998**, *69*, 3357.

- (36) Fauth, J. M.; Schweiger, A.; Braunschweiler, L.; Forrer, J.; Ernst, R. R. *J. Magn. Reson.* **1986**, *66*, 74.
- (37) *MatLab* v.6.1; The MathWorks: Natick, MA, 2001.
- (38) Gromov, I.; Krymov, V.; Manikandan, P.; Arieli, D.; Goldfarb, D. *J. Magn. Reson.* **1999**, *139*, 8.
- (39) Davies, E. R. *Phys. Lett.* **1974**, *47A*, 1.
- (40) Szoenfogel, R.; Goldfarb, D. *Mol. Phys.* **1998**, *95*, 1295.
- (41) Erickson, R. *Chem. Phys.* **1996**, *202*, 263.
- (42) Froncisz, W.; Hyde, J. S. *J. Chem. Phys.* **1980**, *73*, 3123.
- (43) Goldfarb, D.; Kevan, L. *J. Man. Reson.* **1988**, *76*, 276.
- (44) Schweiger, A.; Ernst, R. R. *J. Magn. Reson.* **1988**, *77*, 512.
- (45) Schweiger, A. *Angew. Chem., Int. Ed. Engl.* **1991**, *30*, 265.
- (46) Gemperle, C.; Aebeli, G.; Schweiger, A.; Ernst, R. *J. Magn. Reson.* **1990**, *88*, 241.
- (47) Burghaus, O.; Plato, M.; Rohrer, M.; Möbius, K.; MacMillan, F.; Lubitz, W. *J. Phys. Chem.* **1993**, *97*, 7639.
- (48) Rist, G.; Hyde, J. S. *J. Chem. Phys.* **1968**, *49*, 2449.
- (49) Rohrer, M.; Plato, M.; MacMillan, F.; Grishin, Y.; Lubitz, W.; Möbius, K. *J. Magn. Reson. A* **1995**, *116*, 59.
- (50) Mabbs, F. E.; Porter, J. K. *J. Inorg. Nucl. Chem.* **1973**, *35*, 3219.
- (51) Cannistraro, S. *J. Phys. France* **1990**, *51*, 131.
- (52) Ernst, E.; Freude, D.; Wolf, I. *Chem. Phys. Lett.* **1993**, *212*, 588.
- (53) Grey, C. P.; Vega, A. J. *J. Am. Chem. Soc.* **1995**, *117*, 8232.
- (54) Oka, H.; Tokunaga, Y.; Okada, T.; Ohki, H.; Okuda, T. *Micro-porous Mesoporous Mater.* **1999**, *33*, 257.
- (55) Schoonheydt, R. A. *J. Phys. Chem. Solids* **1989**, *50*, 523.